Coupled-channels description of multinucleon transfer and fusion reactions at energies near and far below the Coulomb barrier

Guillaume Scamps[1,*] and Kouichi Hagino[1,2,3,†]
[1]*Department of Physics, Tohoku University, Sendai 980-8578, Japan*
[2]*Research Center for Electron Photon Science, Tohoku University, 1-2-1 Mikamine, Sendai 982-0826, Japan*
[3]*National Astronomical Observatory of Japan, 2-21-1 Osawa, Mitaka, Tokyo 181-8588, Japan*
(Received 31 August 2015; published 17 November 2015)

We investigate heavy-ion multinucleon transfer reactions using the coupled-channels formalism. We first use the semiclassical approximation and show that a direct coupling between the entrance and the pair transfer channels improves a fit to the experimental one- and two-neutron transfer cross sections for the ^{40}Ca + ^{96}Zr and ^{60}Ni + ^{116}Sn systems. We then discuss the validity of the perturbative approach and highlight the effect of high-order terms. The effect of absorption is also investigated for energies around the Coulomb barrier. Finally, we use a quantal coupled-channels approach to achieve a simultaneous description of the fusion cross sections and the transfer probabilities for the ^{40}Ca + ^{96}Zr reaction. We find a significant effect of the couplings to the collective excited states on the transfer probabilities around the Coulomb barrier.

DOI: 10.1103/PhysRevC.92.054614 PACS number(s): 25.70.Hi, 24.10.Eq, 25.70.Jj

I. INTRODUCTION

A transfer of a few nucleons during the reaction process plays an important role in heavy-ion sub-barrier fusion reactions [1]. The coupling to a transfer degree of freedom is in general weaker than couplings to collective excitations. However, when the coupling is sufficiently large, e.g., for a transfer channel with a positive Q value, it is expected that the transfer coupling leads to an extra enhancement of fusion cross sections below the Coulomb barrier [2–18].

It is well known that two-neutron transfer reactions provide a unique tool to study the pair correlation between nucleons [19–22]. Recently two experiments for heavy-ion transfer reactions have been carried out at energies far below the Coulomb barrier [23,24] in order to study the relation between the transfer of one neutron and that of a pair of neutrons. See also Refs. [25,26]. The experimental data show an enhancement of the two-neutron transfer cross sections compared to a simple estimate based on the independent picture, that is, a square of the transfer probability of one neutron.

Several theoretical studies have been performed in order to understand the reaction dynamics of the pair transfer process. Those include the time-dependent perturbation theory based on the semiclassical approximation [19,20,27–29], the second-order distorted-wave Born approximation (DWBA) [22,30–32], and the semiclassical [26] and the quantal [4,5] coupled-channels approaches. Recently, the time-dependent density functional theory (TDDFT) has also been employed to investigate the transfer reaction. An advantage of this method is that the formalism takes into account simultaneously the structure and the dynamics. Although this method reproduces the individual transfer of nucleons [33–36], the enhancement factor of a two-neutron transfer probability is underestimated with this method [37] even if the pairing correlation is taken into account [38]. This implies a necessity to go beyond the mean-field dynamics with pairing in order to take into account all the remaining correlations [39–42].

In this paper, we carry out a phenomenological study in order to understand the transfer dynamics using the formalism of the semiclassical and the quantal coupled-channels approaches. Our aim in this paper is twofold: One is to understand the reaction dynamics of the two-neutron transfer reactions. We emphasize that the reaction dynamics is so complicated that many microscopic approaches still lack prediction for the two-neutron transfer. In particular, the nature of the two-neutron transfer reaction, that is, the relative importance between the direct and sequential processes, is still under discussion [5,22,27,32,38,43–45]. The second aim of this paper is to describe sub-barrier fusion reactions using the transfer coupling form factors which are consistent with the transfer cross sections. For these purposes, we phenomenologically adjust the parameters in the form factors for the transfer couplings, rather than computing them microscopically.

The paper is organized as follows. In Sec. II, we employ the semiclassical time-dependent coupled-channels method and discuss the sequential and the direct natures of the two-neutron transfer process. In Sec. III, we use the transfer coupling form factors obtained in Sec. II to discuss the role of absorption in the two-neutron transfer reactions. In particular, we investigate the interplay between the transfer and the fusion processes using the quantal coupled-channels approach. We then summarize the paper in Sec. IV.

II. SEMICLASSICAL APPROACH

A. Transfer probability

Since the experimental transfer cross sections are often analyzed using the semiclassical method [19], we first employ it to investigate the nature of the two-neutron transfer.

With the semiclassical approximation to coupled-channels equations, one assumes a Rutherford trajectory for the relative motion $r(t)$ between the colliding nuclei. This yields a

*scamps@nucl.phys.tohoku.ac.jp
†hagino@nucl.phys.tohoku.ac.jp

time-dependent field for the intrinsic motions in the projectile and the target nuclei. That is, the nuclear intrinsic wave function is expanded as $|\Psi(t)\rangle = \sum_{n=0}^{N} c_n(t)|n\rangle$, $n = 0$ corresponding to the entrance channel, and it is then evolved in time as

$$i\hbar\frac{dc_n(t)}{dt} = \sum_{n'} \mathcal{H}_{nn'}(t)\, c_{n'}(t), \tag{1}$$

with $c_n(-\infty) = \delta_{n,0}$. Here, $\mathcal{H}_{nn'}(t)$ is given as

$$\mathcal{H}_{nn'}(t) = \epsilon_n\delta_{n,n'} + V_{nn'}[r(t)], \tag{2}$$

where ϵ_n is the excitation energy for the channel n and $V_{nn'}[r(t)]$ is the coupling form factor evaluated along the classical trajectory, $r(t)$. The probability for the channel n is given as $P_n = |c_n|^2$ at $t = +\infty$.

For the transfer problem, n corresponds to the number of transferred nucleons. By truncating the transfer channels at $n = 2$, the coupling Hamiltonian $\mathcal{H}$ reads

$$\mathcal{H}(t) = \begin{pmatrix} 0 & V_{01}(t) & V_{02}(t) \\ V_{01}(t) & -Q_1 & V_{12}(t) \\ V_{02}(t) & V_{12}(t) & -Q_2 \end{pmatrix}, \tag{3}$$

where $\epsilon_n = -Q_n$ is the transfer Q value for each partition, n. For the coupling form factor $V_{nn'}$, we employ

$$V_{nn'}(r) = \frac{\beta_{nn'}}{\sqrt{4\pi}\, a_{nn'}} \frac{[e^{(r-r_p)/a_{nn'}}]^3}{[1+e^{(r-r_p)/a_{nn'}}]^4}. \tag{4}$$

This function has the exponential form

$$V_{nn'}(r) \sim \frac{\beta_{nn'}}{\sqrt{4\pi}\, a_{nn'}} e^{-(r-r_p)/a_{nn'}} \tag{5}$$

for $r \gg r_p$. Note that this parametrization differs from a frequently used form, $V_{nn'}(r) = \beta_{nn'}\frac{d}{dr}f(r)$, where $f(r)$ is a Fermi function, only for small values of r. We find that the solutions for the coupled-channels equations are numerically more stable with the parametrization given by Eq. (4).

In the actual calculations presented below, we use $r_p = 1.1 \times (A_{\rm T}^{1/3} + A_{\rm P}^{1/3})$ fm, where $A_{\rm T}$ and $A_{\rm P}$ are the mass numbers for the target and the projectile nuclei, respectively. We start the time-dependent Schrödinger equation, Eq. (1), at at an initial distance $r_{\rm ini} = 30$ fm where the coupling is negligible. Following Ref. [29], we evaluate the time dependence of the coupling form factor $V_{nn'}(t)$ by averaging the two Rutherford trajectories, $r_n(t)$ and $r_{n'}(t)$, as $r(t) = (r_n(t) + r_{n'}(t))/2$, where $r_n(t)$ and $r_{n'}(t)$ are evaluated with the energy of $E_n = E_{cm} + Q_n$ and $E_{n'} = E_{cm} + Q_{n'}$, respectively. In order to avoid a dependence of the results on the initial position, $r_{\rm ini}$, all the trajectories are arranged so that the distance of the closest approach is reached at the same time, $t_{\rm min}$. We follow the time evolution until the two fragments are separated with a distance of 30 fm. We have checked that the couplings among the channels are practically negligible after this distance, and thus the transfer probabilities are not altered.

In order to reduce the number of adjustable parameters, we employ two different schemes. The first scheme corresponds to a pure sequential process, for which we set V_{02} to be zero while V_{01} and V_{12} are allowed to be different. On the other hand, the second scheme corresponds to a direct two-neutron transfer process, for which we set $V_{01}(r) = V_{12}(r)$ but $V_{02} \neq 0$ in general. The enhancement of two-neutron transfer process is explained in a different way with these two schemes. In the pure sequential transfer scheme, the enhancement factor is due to the increase of the probability for the transfer of the second neutron after the first neutron is transferred, that is, $|V_{12}| > |V_{01}|$. On the other hand, in the direct transfer scheme, the enhancement is due to the additional coupling between the entrance and the two-neutron transfer channels.

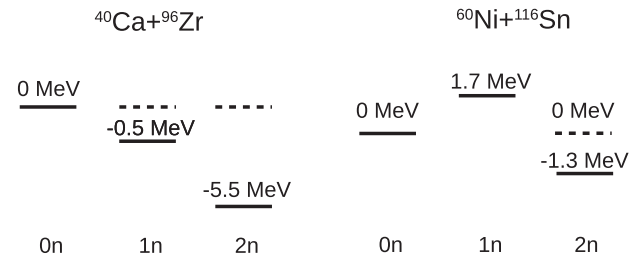

FIG. 1. The ground-state energies for the one-neutron ($1n$) and the two-neutron ($2n$) transfer processes for the ^{40}Ca + ^{96}Zr and ^{60}Ni + ^{116}Sn systems. The dashed lines denote the optimum Q value for each transfer channel.

We test these schemes on the two recent experiments for the ^{40}Ca + ^{96}Zr and ^{60}Ni + ^{116}Sn systems [23,24]. In these references, the experimental data, taken at backward angles in the center-of-mass frame, are given in terms of the transfer probability defined by the ratio of the transfer cross sections to the Rutherford cross sections, $P_{xn} \equiv d\sigma_{xn}/d\sigma_R$, with $x = 1,2,\ldots$, as a function of the distance of the closest approach, D, for the Rutherford trajectory. Figure 1 summarizes the ground-state energies for these systems. The Q value for the ground state to the ground-state transition, $Q_{\rm gg}$, is positive both for the one-neutron and the two-neutron transfer channels for the ^{40}Ca + ^{96}Zr system, while it is negative for the one-neutron transfer and positive for the two-neutron transfer for the ^{60}Ni + ^{116}Sn system.

Let us first consider a case with the ground state to the ground-state Q value, that is, a case with $Q_n = Q_{\rm gg}(n)$, in Eq. (3). We adjust the coefficients $a_{nn'}$ and $\beta_{nn'}$ in Eq. (4) by fitting the experimental data for $D > 13.5$ fm, for which the coupling is weak and only the first-order dynamics is important. Figure 2 shows a comparison of the calculated transfer probabilities so obtained with the experimental data. Those are obtained by varying the center-of-mass energy with fixed values of the scattering angle, that is, $\theta_{\rm c.m.} = 140$ deg for the ^{40}Ca + ^{96}Zr and ^{60}Ni + ^{116}Sn systems. For each energy, the impact parameter is determined so that the scattering angle for the Rutherford trajectory for the entrance channel is consistent with the given value of the scattering angle. In the figure, the thin solid and the dotted lines denote the results with the pure sequential scheme for the $1n$ and $2n$ transfer processes, respectively. On the other hand, the thick solid and the dashed lines denote those with the direct transfer scheme.

The values of the parameters are summarized in Tables I and II for the ^{40}Ca + ^{96}Zr and ^{60}Ni + ^{116}Sn systems, respectively. Notice that the direct two-neutron transfer has a shorter range with small a_2 than the sequential coupling, in accordance

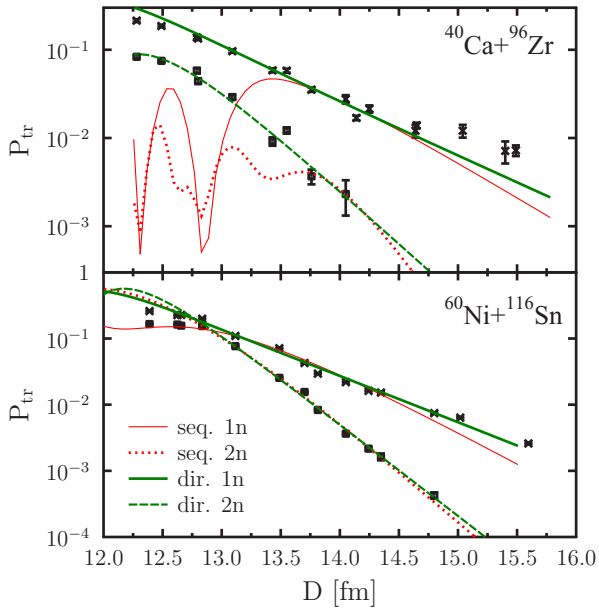

FIG. 2. (Color online) The transfer probabilities for the ^{40}Ca + ^{96}Zr (the upper panel) and ^{60}Ni + ^{116}Sn (the lower panel) reactions as a function of the distance of the closest approach, D, for the Rutherford trajectory. The experimental data, taken form Refs. [23,24], for the one-neutron (the crosses) and the two-neutron (the squares) transfers are compared to transfer probabilities for the ground state to the ground-state transitions obtained with the pure sequential scheme (the thin solid line for the $1n$ transfer and the dotted line for the $2n$ transfer) and with the direct transfer scheme (the thick solid line for the $1n$ transfer and the dashed line for the $2n$ transfer).

with the argument in Ref. [46]. One can also notice that with the sequential scheme one has to take considerably different parameters for V_{12} from those for V_{01} in order to reproduce the experimental two-neutron transfer probability. This may appear unnatural since a drastic change of structure is not expected even after one neutron is transferred, although it may simply mock up a constructive interference of different transfer paths [47].

TABLE I. The parameters for the transfer coupling form factors for the ^{40}Ca + ^{96}Zr reaction. For all the rows, a_1 and β_1 are those for the coupling between the entrance and the $1n$ transfer channels. For the sequential scheme (seq.), a_2 and β_2 are those for the coupling between the $1n$ and the $2n$ transfer channels, that is, $a_2 = a_{12}$ and $\beta_2 = \beta_{12}$. For the direct transfer scheme (dir.), a_2 and β_2 are those for the coupling between the $0n$ and the $2n$ transfer channels, that is, $a_2 = a_{02}$ and $\beta_2 = \beta_{02}$. These parameters are obtained either with the ground state to the ground-state transfer Q values (Q_{gg}) or with the optimum Q values (Q_{opt}).

Q	Scheme	a_1 (fm)	β_1 (MeV fm)	a_2 (fm)	β_2 (MeV fm)
Q_{gg}	seq.	1.015	121.8	0.726	4470
Q_{gg}	dir.	1.309	39.05	0.727	443
Q_{opt}	seq.	1.113	80.33	1.458	107.4
Q_{opt}	dir.	1.230	51.56	0.700	278.9

TABLE II. Same as Table I, but for the ^{60}Ni + ^{116}Sn reaction.

Q	Scheme	a_1 (fm)	β_1 (MeV fm)	a_2 (fm)	β_2 (MeV fm)
Q_{gg}	seq.	0.877	138.9	1.36	131.9
Q_{gg}	dir.	1.18	40.6	0.602	363.4
Q_{opt}	seq.	0.893	126.6	1.38	109.4
Q_{opt}	dir.	1.13	47.1	0.600	384.2

In Fig. 2, an unexpected behavior can be seen for the ^{40}Ca + ^{96}Zr reaction with the pure sequential scheme (the dotted and the thin solid lines). That is, the transfer probabilities oscillate as a function of D, even though the exponential tail is correctly reproduced. This behavior is due to the large Q value for the two-neutron transfer channel, $Q_2 = 5.5$ MeV.

In reality, however, the transfer takes place mainly to excited states, rather than to the ground state [23,48]. In fact, the optimum Q value for a neutron transfer is $Q_{opt} = 0$ [49], and the coupling to the ground state is much weaker [6]. Figure 3 is obtained by using the optimum Q values, that is, $Q = \min(0, Q_{gg})$ (see Fig. 1). See Tables I and II for the parameters. As expected, the agreement with the experimental data is much improved.

In Fig. 3, one can notice that the one-neutron transfer probability is well reproduced with the direct transfer scheme. In contrast, a significant deviation is seen for small values of D with the sequential scheme. This can be attributed to the sequential nature of the transfer dynamics. For large values of D, the transfer probabilities are small and the sequential transfer to the $2n$ channel does not modify P_1. However, as D decreases, the two-step process becomes significant, reducing the probability for the one-neutron transfer channel. With the direct two-neutron transfer scheme, on the other hand, the two-neutron transfer takes place mainly from the entrance

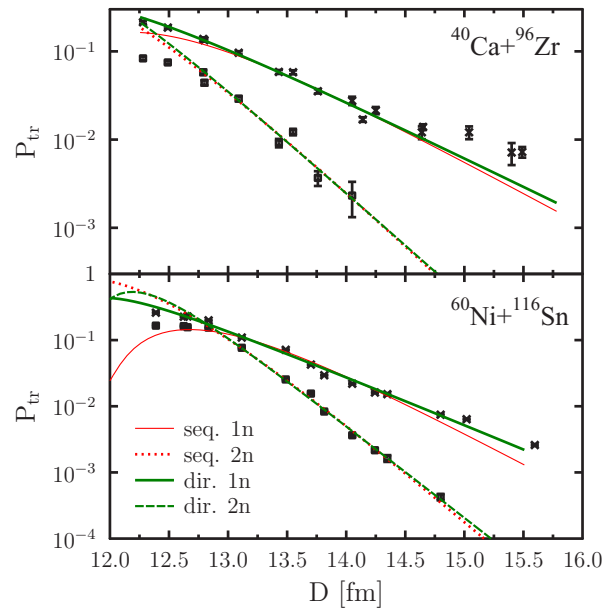

FIG. 3. (Color online) Same as Fig. 2, but with the optimum Q values (see the text).

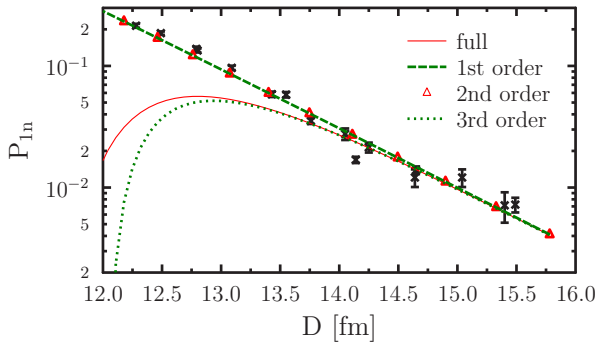

FIG. 4. (Color online) The one-neutron transfer probability as a function of the distance of the closest approach for the ^{40}Ca + ^{96}Zr reaction. The sequential two-neutron scheme with the optimum Q value is employed. The dashed line, the triangles, and the dotted line are the results of the time-dependent perturbation theory with the first, the second, and the third orders, respectively. Those results are compared to the exact solution (the solid line) and to the experimental data (the crosses). The coupling parameters used here are $a_1 = 1.55$ fm, $\beta_1 = 26.4$ MeV fm, $a_2 = 1.286$ fm, and $\beta_2 = 150.4$ MeV fm.

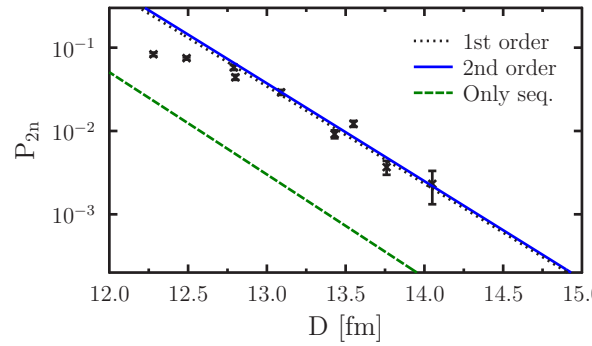

FIG. 5. (Color online) The two-neutron transfer probability for the ^{40}Ca + ^{96}Zr system as a function of the distance of the closest approach, D. The direct two-neutron transfer scheme with the optimum Q values is employed. The results of the time-dependent perturbation theory up to the first and the second orders are shown by the dotted and the solid lines, respectively. The result of the second-order calculation neglecting the direct two-neutron transfer couplings is also shown by the dashed line (see text). The experimental data are taken from Ref. [23].

channel (see Sec. II C below), as the coupling between the $1n$ and the $2n$ channels stays relatively weak.

In order to better understand this phenomena, one can use the time-dependent perturbation theory by separating the contribution of each order. Figure 4 shows the approximate solutions for the one-neutron transfer reaction for the ^{40}Ca + ^{96}Zr system obtained with the sequential two-neutron scheme. Here, the coupling parameters are readjusted in order to reproduce the experimental data for large D with the first-order dynamics. Up to the first order, the one-neutron transfer probability is found to be exponential with the distance of the closest approach in the whole range of D shown in the figure. As a consequence, the calculation appears to be consistent with the experimental data. This remains to be the same up to the second order, since there is no second-order contribution to the one-neutron transfer channel. On the other hand, if one considers up to the third order, the result is drastically changed and becomes close to the full-order result obtained by solving the time-dependent coupled-channels equations, Eq. (1), without using the perturbation theory. That is, the third-order process now includes the diminution of the one-neutron transfer probability due to the second-order process to the $2n$ channel. From this comparison, we can conclude that the perturbative calculations must be used with caution for an application to multinucleon transfer calculations, since a good agreement with experimental data may be an artifact of the first-order perturbation theory.

Notice that the sequential scheme largely underestimates the transfer probabilities at small D. In this region, the absorption effect would be important, but the effect of absorption will always decrease the transfer probabilities, as we discuss in Sec. II C. Evidently, a pure sequential two-neutron transfer is not compatible with the experimental data, at least with this simple model. See also Refs. [5,44] for a similar conclusion. We have confirmed that this conclusion remains the same even if we include a few states around the optimum Q value for each transfer partition.

Notice that the semiclassical transfer calculations have indicated that the two-neutron transfer process occurs predominantly with a sequential process [27–29]. The present result is somewhat in contradiction with the previous finding of the semiclassical method. The difference may be due to the fact that the previous semiclassical calculations take into account many intermediate $1n$ transfer channels with a wide distribution of excitation energy while we include only a single channel (or at most a few channels). In this sense, our coupling scheme may have to be regarded as an effective one, which implicitly takes into account the effect of many other intermediate channels. It would be an interesting future work to clarify how the elimination of the intermediate states gradually changes the nature of the two-neutron transfer couplings.

B. Nature of two-neutron transfer

In the previous subsection, we have argued that the direct two-neutron transfer scheme is more plausible than the purely sequential transfer scheme as long as a simple coupling scheme as in Eq. (3) is employed. Let us then investigate the nature of the two-neutron transfer process by assuming the direct transfer scheme with the optimum Q values. Figure 5 shows the result for the probability of the two-neutron channel for the ^{40}Ca + ^{96}Zr system obtained by the perturbation theory. To this end, we use the same parameters as those used in Fig. 3. The dotted line denotes the result of the first-order perturbation theory, which includes only the direct population of the $2n$ transfer channel from the entrance channel. The solid line, on the other hand, denotes the result of the second-order perturbation theory, which in addition includes the sequential two-neutron transfer via the intermediate $1n$ transfer channel. For a comparison, the figure also shows the calculation with the second-order contribution only (the dashed line), that is, the calculation neglecting the direct two-neutron coupling.

One can see that the sequential process is negligibly small as compared to the first-order process. That is, the two-neutron transfer in this model is largely dominated by the direct two-neutron transfer from the entrance channel partition. Notice that this conclusion is a direct consequence of the simplified transfer model with the choice of $V_{12}(r) = V_{01}(r)$, and it would need to be confirmed with a more general model.

C. Effect of absorption

While the experimental data for the two-neutron transfer are well described with the direct two-neutron transfer scheme for the distance of the closest approach of 13 fm or larger, a discrepancy is found for $D < 13$ fm (except for the ^{40}Ca + ^{96}Zr system with Q_{gg}). While the calculations predict a nearly exponential behavior of D, the experimental data show a much slower dependence in this region. This could be attributed to several mechanisms beyond the present model, such as a deviation of the classical trajectory from the Rutherford trajectory, a loss of one-to-one correspondence between the experimental and the theoretical definitions of the transfer probabilities (that is, the quantity $d\sigma_{xn}/d\sigma_R$ may not be able to be interpreted as a transfer probability at small values of D), and a deviation of the coupling form factor from that given by Eq. (4).

In the following, we choose to test a hypothesis that this effect originates from the absorption of the wave function, which corresponds to a capture and/or inelastic excitations. In order to take into account this effect in a simple way, we add an imaginary potential to the diagonal part of the Hamiltonian, Eq. (3), with the expression

$$iW(r) = \frac{-iW_0}{1 + \exp[(r - R_W)/a_W]}, \tag{6}$$

for which the parameters W_0, R_W, and a_W may be different for each channel. We adjust these parameters in order to reproduce the experimental transfer probabilities using the direct two-neutron transfer scheme with the optimum Q values. The resultant values for the parameters are summarized in Table III, and the fit to the experimental transfer probabilities is shown in Fig. 6. One can see that a good agreement between the calculations and the experimental data is achieved, including the region with small values of the distance of the closest approach, although the good reproduction of the data may be due to the large number of adjustable parameters.

The single-channel calculations with those absorbing potentials lead to the survival probability for each channel shown in Fig. 7. Notice that this is not the survival probability for the whole transfer process, that is, $P_{\rm surv} = |c_0|^2 + |c_1|^2 + |c_2|^2$, but the single-channel probability corresponding to that given

TABLE III. The parameters of the absorbing potential for each channel required to fit the experimental data.

System	Channel	W_0 (MeV)	R_W (fm)	a_W (fm)
^{40}Ca + ^{96}Zr	0n and 1n	9.96	11.88	0.12
	2n	9.89	12.10	0.18
^{60}Ni + ^{116}Sn	0n and 1n	10.03	12.01	0.08
	2n	10.08	12.25	0.16

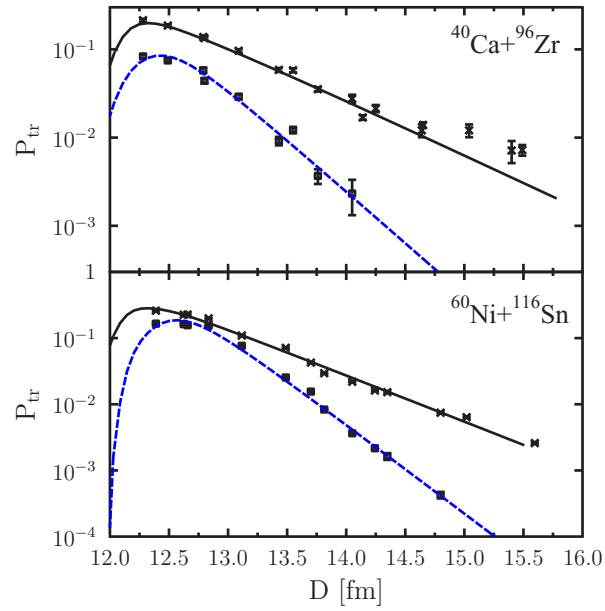

FIG. 6. (Color online) The transfer probabilities as a function of the distance of the closest approach, D, calculated by including the effect of absorption of the classical trajectories with the imaginary potential. The direct two-neutron transfer scheme with the optimum Q value is employed. The solid lines denote the results for the one-neutron transfer process, while the dashed lines are for the two-neutron transfer process. The experimental data are taken from Refs. [23,24].

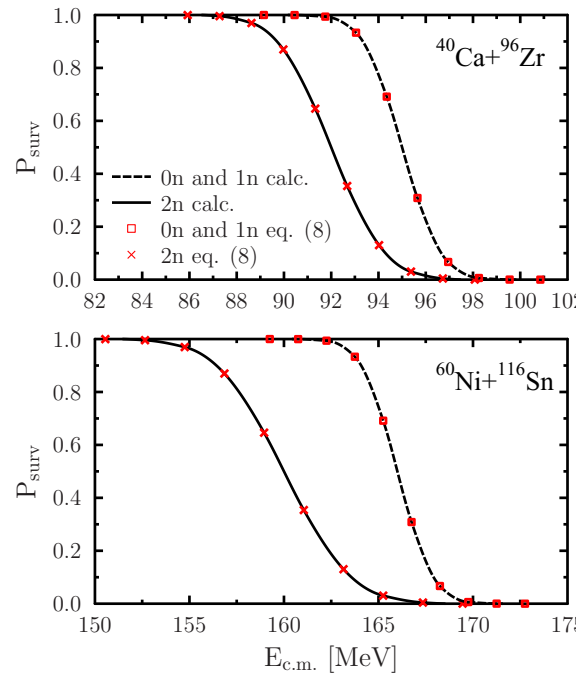

FIG. 7. (Color online) The s-wave survival probability for each channel as a function of the center of mass energy. It is obtained by solving the time-dependent Schrödinger equation with a single channel including the imaginary potential. The crosses and the squares show a fit with the complementary error function given by Eq. (8).

TABLE IV. The parameters for the complementary error function given by Eq. (8) which fit the results of the time-dependent calculations for the survival probability for each channel.

System	Channel	B (MeV)	σ (MeV)
^{40}Ca + ^{96}Zr	$0n$	95	1.3
	$1n$	95	1.3
	$2n$	92	1.8
^{60}Ni + ^{116}Sn	$0n$	166	1.3
	$1n$	166	1.5
	$2n$	160	2.8

by [29]

$$P_{\rm surv}^{(xn)}(E) = 1 - \exp\left(\frac{2}{\hbar}\int_0^\infty W[r_n(t)]dt\right). \quad (7)$$

We find that the survival probability for each channel, $P_{\rm surv}^{(xn)}$, can be well parametrized with the complementary error function,

$$P_{\rm surv}^{(xn)}(E) \sim \frac{1}{2} + \frac{1}{2}{\rm erfc}\left(\frac{E-B}{\sqrt{2}\sigma}\right), \quad (8)$$

with the parameters given in Table IV (see Fig. 7). Notice that the values of the parameters are considerably different between the two-neutron transfer channel and the one-neutron transfer channel. The meaning of the imaginary potential is to take into account the loss of flux from the model space explicitly taken into account in the calculations to the outside, which include the tunneling through the barrier (that is, the capture) and the inelastic processes. In either case, the imaginary potential reduces the transfer probabilities. The different values of the parameters for each channel implies that the effect of absorption may be different in each channel. We find that it is essential to have the channel dependence in the parameters of the absorbing potential in order to account for the diminution of the $2n$ transfer probability without significantly degrading the reproduction of the $1n$ transfer channel.

III. QUANTAL COUPLED-CHANNELS APPROACH

We have shown in the previous section that the role of absorption may differ among the different transfer channels. We have achieved this conclusion using the semiclassical method. A drawback of the semiclassical method is that the tunneling process is not easily described with it, although one may still do it using the time evolution along the imaginary time axis [50,51]. For this reason, in this section, we use the full quantal coupled-channels approach, which can also be applied to a simultaneous description of fusion cross sections and transfer probabilities.

The coupled-channels equations for a total angular momentum J read [50]

$$\left[-\frac{\hbar^2}{2\mu}\frac{d^2}{dr^2} + \frac{J(J+1)\hbar^2}{2\mu r^2} + V_N(r) + iW_N(r) + \frac{Z_P Z_T e^2}{r} + \epsilon_n - E\right]u_n(r) + \sum_m V_{nm}(r)u_m(r) = 0, \quad (9)$$

TABLE V. The parameters for the nuclear potential used in the coupled-channels calculations for each system.

System	V_0 (MeV)	r_0 (fm)	a_0 (fm)	W_0 (MeV)	r_W (fm)	a_W (fm)
^{40}Ca + ^{96}Zr	87.0	1.13	0.700	40	1.1	0.2
^{60}Ni + ^{116}Sn	80.0	1.1	0.487	20	0.9	0.487

where μ is the reduced mass, E is the center-of-mass energy, and Z_P and Z_T are the charge numbers of the projectile and the target, respectively. We have used the isocentrifugal approximation [50] and assumed that the angular momentum does not change for each channel. We use a Woods-Saxon parametrization for the nuclear potential, V_N, that is,

$$V_N(r) = \frac{-V_0}{1 + \exp[(r - R_0)/a_0]} \quad (10)$$

with $R_0 = r_0(A_P^{1/3} + A_T^{1/3})$. We use the Woods-Saxon parametrization also for the imaginary potential, W_N, as in Eq. (6).

We solve the coupled-channels equations using a modified version of the computer program CCFULL [52] in order to construct the transfer cross sections from the S matrix. The transfer probability is then calculated using the same definition as the experimental probability, that is, $P_{xn} \equiv d\sigma_{xn}/d\sigma_R$.

A. Quantum effect

Let us first solve the coupled-channels equations including only the transfer channels and examine the validity of the semiclassical trajectory approximation. To this end, we use the direct two-neutron transfer scheme with the optimum Q values, for which the parameters for the transfer coupling form factors are given in Tables I and II. We use the parameters in Table V for the nucleus-nucleus potential (both for the real and the imaginary parts). In order to simplify the comparison between the semiclassical and the quantal calculations, we neglect the effect of absorption on the transfer probabilities. For this purpose, the real and the imaginary parts of the nuclear potential are not taken into account in the semiclassical calculation. Moreover, we choose the parameters of the nuclear potential so that they yield a higher barrier than the systematics.

Figure 8 shows a comparison between the quantal coupled-channels calculations and the semiclassical coupled-channels calculations for the same coupling potentials. One can find a good agreement between the two calculations for the distance of the closest approach of $D > 13.5$ fm; that is, the two calculations differ only by about 10%. The difference between the two calculations is more significant for $D < 13$ fm, where the quantum effect as well as the absorption process play an important role.

Evidently, the conclusions obtained in the previous section with the semiclassical method remain unchanged even if we use the quantal coupled-channels method.

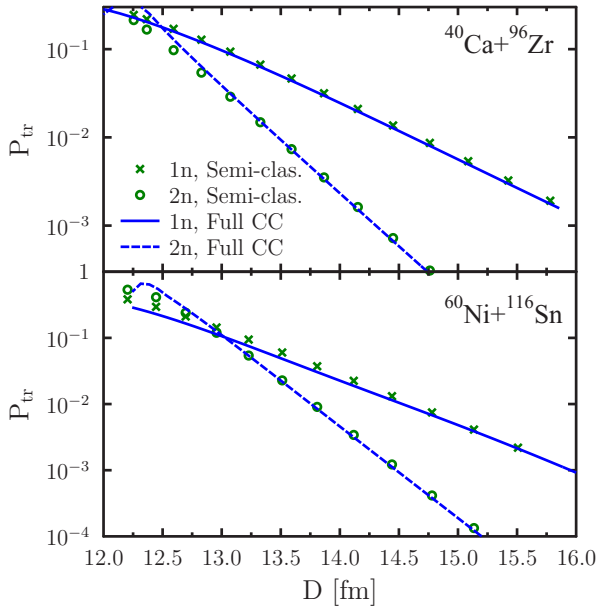

FIG. 8. (Color online) A comparison between the transfer probabilities obtained with the semiclassical approximation (the crosses and the circles) and those with the quantal coupled-channels calculations (the solid and the dashed lines) for the $^{40}\mathrm{Ca}+{}^{96}\mathrm{Zr}$ and $^{60}\mathrm{Ni}+{}^{116}\mathrm{Sn}$ systems.

B. Role of absorption

We next discuss the role of absorption in the transfer reactions by fully taking into account the tunneling effect. For this purpose, we still use the three-channel problem in the previous subsection. Figure 9 compares two calculations for the transfer probabilities for the $^{60}\mathrm{Ni}+{}^{116}\mathrm{Sn}$ system. The first

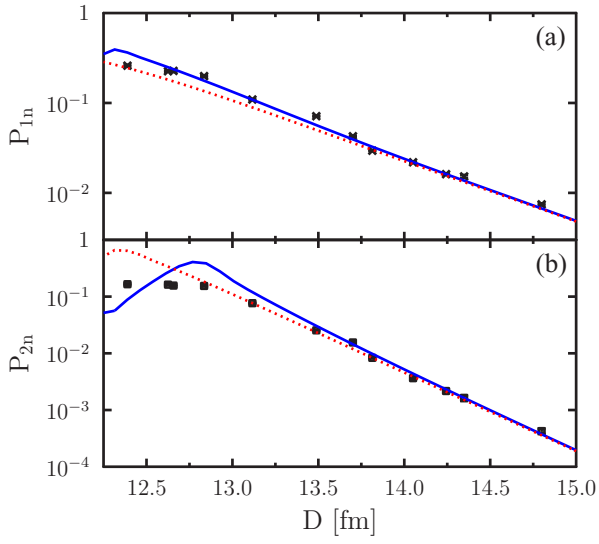

FIG. 9. (Color online) The one-neutron transfer (the upper panel) and the two-neutron transfer (the lower panel) probabilities as a function of the distance of the closest approach for the $^{60}\mathrm{Ni}+{}^{116}\mathrm{Sn}$ reaction. The solid and the dotted lines are obtained with the nuclear potential, which yields the barrier heights of $B = 166$ and 179.9 MeV, respectively.

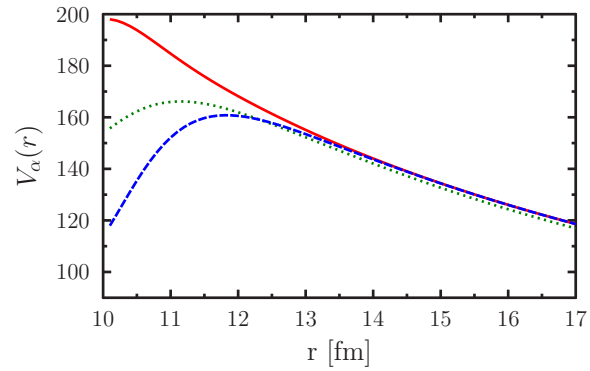

FIG. 10. (Color online) The three eigenbarriers obtained by diagonalizing the intrinsic Hamiltonian matrix, Eq. (3), at each internuclear separation, r.

calculation shown by the dotted line is the same as the dashed line in Fig. 8. This result is obtained with the nuclear potential of Table V, which yields the barrier height of $B = 179.9$ MeV. Notice that the Broglia-Winther potential [29] leads to a somewhat lower barrier height, that is, $B = 166$ MeV. We therefore repeat the transfer calculations using the potential with $V_0 = 116$ MeV, $r_0 = 1.2$ fm, and $a_0 = 0.687$ fm, which yields the same barrier height as the Broglia-Winther potential. The result so obtained is denoted by the solid line in the figure. One can see that the one-neutron transfer cross sections do not differ much between the two calculations. In contrast, it is interesting to notice that the two-neutron transfer cross sections are considerably affected by the choice of the nuclear potential. Notice that we use the same imaginary potential for all the channels. Even so, we reach the same conclusion as in Fig. 6, that is, the $2n$ transfer amplitude is more absorbed than the $1n$ transfer amplitude. In this case, the absorption is more likely due to the capture rather than the inelastic processes.

In order to understand a reasoning for this phenomenon, Fig. 10 shows the eigenbarriers by diagonalizing the coupling matrix, Eq. (3), at each position r. That is,

$$V_\alpha(r) = V_N(r) + \frac{Z_P Z_T e^2}{r} + \lambda_\alpha(r), \tag{11}$$

where $\lambda_\alpha(r)$ is an eigenvalue of the coupling matrix. In general, the eigenvectors depend on the position r [50]. However, for the direct two-neutron transfer scheme with $V_{01} = V_{12}$ and $Q_2 = 0$, one of the eigenvectors becomes independent of r. This special eigenvector has a structure of $|\psi_1\rangle = \frac{1}{\sqrt{2}}(|0n\rangle - |2n\rangle)$ with the eigenvalue of $-V_{02}(r)$. Notice that the $1n$ channel does not contribute to this eigenstate. The other two eigenstates are given as a liner superposition of all the three channels, $|0n\rangle$, $|1n\rangle$, and $|2n\rangle$. For a positive value of the ratio β_{02}/a_{02}, that is the case in our calculations, the eigenbarrier corresponding to the state $|\psi_1\rangle$ provides the lowest barrier among the three eigenbarriers and is shown by the dashed line in Fig. 10. This implies that the capture occurs more easily from the $2n$ channel as compared to the $1n$ channel due to the lowest eigenbarrier, in which the $1n$ channel is absent.

As we discuss in the next section, the nonreproduction of the experimental probabilities in the vicinity of the barrier

TABLE VI. The Coulomb deformation parameter, β_C, the nuclear deformation parameter, β_N, the multipolarity and the parity, λ^π, and the excitation energy E for the collective states included in the coupled-channels calculations. The radius parameter of $r_0 = 1.2$ fm is used in the coupling potentials.

Nucleus	λ^π	β_C	β_N	E (MeV)
^{40}Ca	3^-	0.43	0.43	3.737
^{96}Zr	3^-	0.27	0.305	1.89

shown in Fig. 9 may be attributed to the fact that we do not include the excited collective states in these calculations.

C. Simultaneous description of fusion and multineutron transfer

One of the most important issues in the study of transfer reactions is to investigate whether the same strengths for the transfer couplings simultaneously account for fusion and transfer cross sections. Such attempt has been successfully made for the ^{33}S + ^{90,91,92}Zr systems [53,54]. We make here a similar attempt for the ^{40}Ca + ^{96}Zr reaction, for which fusion cross sections have been measured with high precision [7,8]. To this end, we include both the multineutron transfer channels and the collective inelastic channels in the coupled-channels equations. To be more specific, we take into account the one octupole phonon excitation in ^{40}Ca as well as the octupole phonon excitations in ^{96}Zr up to the three-phonon states. We include all the possible mutual excitations. The parameters for the collective couplings are given in Table VI. The deformation parameters for the Coulomb couplings are estimated with the measured $B(E3)$ values, while we slightly increase the nuclear deformation parameter for ^{96}Zr in order to better reproduce the experimental data. The multineutron transfer channels are taken into account up to three-neutron transfer, with the method of Esbensen and Landowne [4]. That is, we treat the collective excitations and the transfer channels as independent degrees of freedom so that the channel wave functions are specified as $|n_{\rm tr} n_{\rm inel}\rangle$, where $n_{\rm tr}$ (=0, 1, 2, and 3) indicates the number of transferred neutrons while $n_{\rm inel}$ specifies the inelastic channels. This lead to the total number of 32 channels (=2 × 4 × 4, where the 2 is for the excitation in ^{40}Ca, the first 4 is for the excitations in ^{96}Zr, and the last 4 is for the transfer channels). For the one- and the two-neutron transfers, the parameters for the transfer couplings are readjusted to fit the measured transfer probabilities with the direct two-neutron transfer scheme with the optimum Q values, that is, $Q = 0$. The resultant coupling coefficients are $\beta_{01} = -71$ MeV fm, $a_{01} = 1.13$ fm, $\beta_{02} = -105$ MeV fm, and $a_{02} = 0.82$ fm. The three-neutron transfer channel is included with the coupling $V_{23} = V_{01}$, $V_{13} = V_{02}$, and $V_{03} = 0$. We employ $Q_3 = +4$ MeV in order to reproduce the experimental data for the three-neutron transfer reaction. We use the nucleus-nucleus potential given in Table V.

Figures 11(a) and 11(b) show the results of the coupled-channels calculations so obtained for the fusion cross sections $\sigma_{\rm f}$ and the fusion barrier distributions $D_{\rm fus}$ for the ^{40}Ca + ^{96}Zr system, respectively. Here, the fusion barrier distribution is

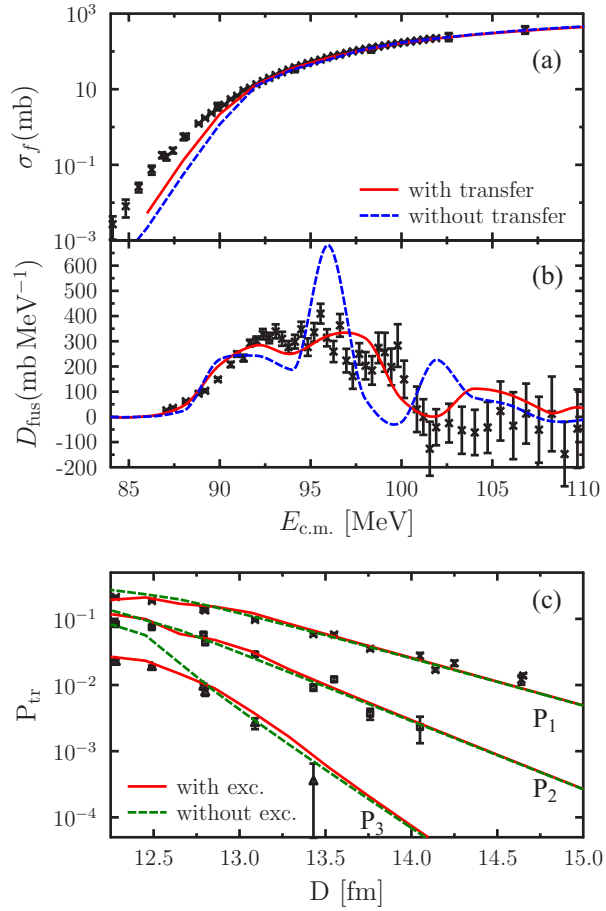

FIG. 11. (Color online) (a) The fusion cross sections for the ^{40}Ca + ^{96}Zr reaction. The dashed line shows the results of the coupled-channels calculations including only the collective excitations in the colliding nuclei, while the solid line shows those with both the inelastic and the multineutron transfer channels. (b) The corresponding fusion barrier distribution. The experimental data are taken from Refs. [7,8]. (c) The probabilities for the multineutron transfer reactions obtained with (the solid lines) and without (the dashed lines) taking into account the inelastic excitations. The experimental data are taken from Ref. [23].

defined as $D_{\rm fus} = d^2(E\sigma_{\rm f})/dE^2$ [55,56]. In the figures, the dashed lines denote the results obtained by including only the inelastic excitation in the colliding nuclei, while the solid lines are obtained by including in addition the multineutron transfer couplings. One can see that both the fusion cross sections and the barrier distributions are well reproduced by including the multineutron transfer channels, although fusion cross sections are still underestimated at low energies. In particular, the flatness of fusion barrier distribution is well reproduced by this calculation. We do not know the origin for the underestimation of fusion cross sections at low energies, but a similar tendency is seen also in another coupled-channels calculation reported in Ref. [46]. This could be due to the absence of other transfer channels, such as proton and α particle transfers, or the change in the collective couplings for the transfer channels.

The transfer probabilities are shown in Fig. 11(c). The solid lines show the results of the full coupled-channels calculations,

while the dashed lines are obtained by excluding the inelastic channels, that is, by including only the multineutron transfer channels. One can see that the inelastic excitations do not affect the one- and two-neutron transfer channels much, but the three-neutron transfer channel is sensitive to the inelastic excitations, especially for $D < 13$ fm. One can also see that the present coupled-channels calculations well reproduce the experimental data for the transfer probabilities. It is worthwhile to mention that the fusion cross sections and the transfer probabilities are reproduced simultaneously within a single framework.

IV. SUMMARY

We have carried out a phenomenological study on the heavy-ion multineutron transfer reactions using the coupled-channels approaches. The aim was to adjust the parameters for the transfer couplings using the experimental data at energies far below the Coulomb barrier, where the perturbation treatment is applicable, and to investigate the dynamics at energies around the barrier, where the higher order terms as well as the absorption are important. We have applied this strategy to the ^{40}Ca + ^{96}Zr and ^{60}Ni + ^{116}Sn systems, for which the transfer probabilities were recently measured. We have first used the semiclassical approximation to a three-channel problem with one- and two-neutron transfer channels and have obtained the following conclusions: (i) the inclusion of the direct coupling between the entrance channel and the two-neutron transfer channel is necessary in order to reproduce the experimental data, (ii) the higher order dynamics is important at energies around the Coulomb barrier and the first-order treatment may not be sufficient, (iii) the absorption has an important effect on the transfer probabilities at energies around the Coulomb barrier, and (iv) the absorption plays a more important role for the two-neutron transfer channel as compared to the one-neutron transfer channel.

The role of absorption has been confirmed also by using the quantal coupled-channels method for the ^{60}Ni + ^{116}Sn system. For the ^{40}Ca + ^{96}Zr system, we have succeeded in reproducing simultaneously the fusion cross sections, the fusion barrier distribution, and the transfer probabilities up to the three-neutron transfer channel, by including both the collective excitations and the transfer channels in the coupled-channels calculations.

There have not been many systems for which both the fusion and the multineutron transfer cross sections are available at energies around and far below the Coulomb barrier. In that sense, the present phenomenological analysis is somewhat limited. It would be interesting to test the present approach to future experimental data for fusion and multineutron transfer reactions.

ACKNOWLEDGMENTS

We thank D. Lacroix, D. Montanari, L. Corradi, and A. Vitturi for useful discussions. G.S. thanks also G. Adamian and N. Antonenko for useful discussions. G.S. acknowledges the Japan Society for the Promotion of Science for the JSPS postdoctoral fellowship for foreign researchers. This work was supported by Grant-in-Aid for JSPS Fellows No. 14F04769.

[1] C. L. Jiang, K. E. Rehm, B. B. Back, H. Esbensen, R. V. F. Janssens, A. M. Stefanini, and G. Montagnoli, Phys. Rev. C **89**, 051603(R) (2014).
[2] R. A. Broglia, C. H. Dasso, S. Landowne, and A. Winther, Phys. Rev. C **27**, 2433(R) (1983).
[3] S. Y. Lee, Phys. Rev. C **29**, 1932 (1984).
[4] H. Esbensen and S. Landowne, Nucl. Phys. A **492**, 473 (1989).
[5] H. Esbensen, C. L. Jiang, and K. E. Rehm, Phys. Rev. C **57**, 2401 (1998).
[6] V. I. Zagrebaev, Phys. Rev. C **67**, 061601(R) (2003).
[7] H. Timmers *et al.*, Phys. Lett. B **399**, 35 (1997); Nucl. Phys. A **633**, 421 (1998).
[8] A. M. Stefanini *et al.*, Phys. Lett. B **728**, 639 (2014).
[9] A. M. Stefanini, B. R. Behera, S. Beghini, L. Corradi, E. Fioretto, A. Gadea, G. Montagnoli, N. Rowley, F. Scarlassara, S. Szilner, and M. Trotta, Phys. Rev. C **76**, 014610 (2007).
[10] A. M. Stefanini *et al.*, Eur. Phys. J. A **49**, 63 (2013).
[11] D. Bourgin, S. Courtin, F. Haas, A. M. Stefanini, G. Montagnoli, A. Goasduff, D. Montanari, L. Corradi, E. Fioretto, J. Huiming, F. Scarlassara, N. Rowley, S. Szilner, and T. Mijatovic, Phys. Rev. C **90**, 044610 (2014).
[12] Z. Kohley, Z. Kohley, J. F. Liang, D. Shapira, C. J. Gross, R. L. Varner, J. M. Allmond, J. J. Kolata, P. E. Mueller, and A. Roberts, Phys. Rev. C **87**, 064612 (2013).
[13] H. Q. Zhang, C. J. Lin, F. Yang, H. M. Jia, X. X. Xu, Z. D. Wu, F. Jia, S. T. Zhang, Z. H. Liu, A. Richard, and C. Beck, Phys. Rev. C **82**, 054609 (2010).
[14] H. M. Jia, C. J. Lin, F. Yang, X. X. Xu, H. Q. Zhang, Z. H. Liu, Z. D. Wu, L. Yang, N. R. Ma, P. F. Bao, and L. J. Sun, Phys. Rev. C **89**, 064605 (2014).
[15] V. A. Rachkov, A. V. Karpov, A. S. Denikin, and V. I. Zagrebaev, Phys. Rev. C **90**, 014614 (2014).
[16] V. V. Sargsyan, G. G. Adamian, N. V. Antonenko, W. Scheid, and H. Q. Zhang, Phys. Rev. C **84**, 064614 (2011).
[17] V. V. Sargsyan, G. G. Adamian, N. V. Antonenko, W. Scheid, and H. Q. Zhang, Phys. Rev. C **86**, 014602 (2012).
[18] V. V. Sargsyan, G. Scamps, G. G. Adamian, N. V. Antonenko, and D. Lacroix, Phys. Rev. C **88**, 064601 (2013).
[19] W. von Oertzen and A. Vitturi, Rep. Prog. Phys. **64**, 1247 (2001).
[20] A. Vitturi and H. M. Sofia, Prog. Theo. Phys. Suppl. **196**, 72 (2012).
[21] S. Yoshida, Nucl. Phys. **33**, 685 (1962).
[22] G. Potel, A. Idini, F. Barrando, E. Vigezzi, and R. A. Broglia, Rep. Prog. Phys. **76**, 106301 (2013).
[23] L. Corradi *et al.*, Phys. Rev. C **84**, 034603 (2011).
[24] D. Montanari *et al.*, Phys. Rev. Lett. **113**, 052501 (2014).
[25] S. Szilner *et al.*, Phys. Rev. C **76**, 024604 (2007).
[26] L. Corradi, G. Pollarolo, and S. Szilner, J. Phys. G **36**, 113101 (2009).
[27] R. A. Broglia, U. Götz, M. Ichimura, T. Kammuri, and A. Winther, Phys. Lett. B **45**, 23 (1973).
[28] E. Maglione, G. Pollarolo, A. Vitturi, R. A. Broglia, and A. Winther, Phys. Lett. **162B**, 59 (1985).

[29] R. A. Broglia and A. Winther, *Heavy Ion Reactions* (Addison-Wesley, Redwood City, CA, 1991).
[30] G. Potel, F. Barranco, F. Marini, A. Idini, E. Vigezzi, and R. A. Broglia, Phys. Rev. Lett. **107**, 092501 (2011).
[31] G. Potel, A. Idini, F. Barranco, E. Vigezzi, and R. A. Broglia, Phys. Rev. C **87**, 054321 (2013).
[32] B. F. Bayman and J. Chen, Phys. Rev. C **26**, 1509 (1982).
[33] C. Simenel, Phys. Rev. Lett. **105**, 192701 (2010).
[34] A. S. Umar, V. E. Oberacker, and J. A. Maruhn, Eur. Phys. J. A **37**, 245 (2008).
[35] K. Sekizawa and K. Yabana, Phys. Rev. C **88**, 014614 (2013); **90**, 064614 (2014).
[36] M. Evers, M. Dasgupta, D. J. Hinde, D. H. Luong, R. Rafiei, R. du Rietz, and C. Simenel, Phys. Rev. C **84**, 054614 (2011).
[37] G. Scamps and D. Lacroix, EPJ Web Conf. **86**, 00042 (2015).
[38] G. Scamps and D. Lacroix, Phys. Rev. C **87**, 014605 (2013).
[39] C. Simenel, Phys. Rev. Lett. **106**, 112502 (2011).
[40] K. Washiyama, S. Ayik, and D. Lacroix, Phys. Rev. C **80**, 031602(R) (2009).
[41] S. Ayik, O. Yilmaz, B. Yilmaz, A. S. Umar, A. Gokalp, G. Turan, and D. Lacroix, Phys. Rev. C **91**, 054601 (2015).
[42] C.-Y. Wong and H. H. K. Tang, Phys. Rev. Lett. **40**, 1070 (1978).
[43] T. Kammuri, Nucl. Phys. A **259**, 343 (1976).
[44] A. Parmar, Nucl. Phys. A **940**, 167 (2015).
[45] P. K. Sahu, R. K. Choudhury, D. C. Biswas, and B. K. Nayak, Phys. Rev. C **64**, 014609 (2001).
[46] H. Esbensen and A. M. Stefanini, Phys. Rev. C **89**, 044616 (2014).
[47] J. A. Lay, L. Fortunato, and A. Vitturi, Phys. Rev. C **89**, 034618 (2014).
[48] N. Rowley, in *the Proceedings of the International Workshop on Fusion Dynamics at the Extremes*, edited by Yu. Ts. Oganessian and V. I. Zagrebaev (World Scientific, Singapore, 2001), p. 296.
[49] W. Henning, Y. Eisen, H.-J. Körner, D. G. Kovar, J. P. Schiffer, S. Vigdor, and B. Zeidman, Phys. Rev. C **17**, 2245 (1978).
[50] K. Hagino and N. Takigawa, Prog. Theo. Phys. **128**, 1061 (2012).
[51] N. Takigawa, K. Hagino, and M. Abe, Phys. Rev. C **51**, 187 (1995).
[52] K. Hagino, N. Rowley, and A. T. Kruppa, Comp. Phys. Commun. **123**, 143 (1999).
[53] L. Corradi *et al.*, Z. Phys. A **335**, 55 (1990).
[54] L. Corradi *et al.*, Z. Phys. A **346**, 217 (1993).
[55] N. Rowley, G. R. Satchler, and P. H. Stelson, Phys. Lett. B **254**, 25 (1991).
[56] M. Dasgupta, D. J. Hinde, N. Rowley, and A. M. Stefanini, Annu. Rev. Nucl. Part. Sci. **48**, 401 (1998).